Lateral in-plane coupling between graphene nanoribbons: A density functional study

Jianhua Zhao,[1] Xianqi Dai,[1,a)] Yawei Dai,[1] Bao Zhao,[1] and Maohai Xie[2]
[1]*College of Physics & Information Engineering, Henan Normal University, Xinxiang, Henan 453007, People's Republic of China*
[2]*Physics Department, The University of Hong Kong, Hong Kong, People's Republic of China*

(Received 7 October 2011; accepted 23 January 2012; published online 27 February 2012)

Properties brought about by lateral in-plane coupling between graphene nanoribbons (GNRs) are investigated using the first-principle total energy calculations. It is found that, when two GNRs approach each other, the lateral coupling between the two brings about edge state splitting. Between zigzag-edged graphene nanoribbons (ZGNRs), the coupling mainly results from Coulomb and spin-spin interaction, while for armchair-edged graphene nanoribbons (AGNRs), it is from Coulomb interaction only. It is further found that the maximum inter-ribbon distance for effective coupling depends on the type of ribbons, which is ~10 Å for ZGNRs, but ~6 Å for AGNRs. Also, displacements of the GNRs along the ribbon direction are found to affect the electronic properties of the coupled GNRs. The results may be important for the microminiaturization of future nanoelectronic and spintronic devices based on graphene. © *2012 American Institute of Physics*. [doi:10.1063/1.3686673]

I. INTRODUCTION

Since its isolation by scotch tapes, graphene, a single graphite layer, has attracted a broad research interest, due to its superior physical and chemical properties.[1] Graphene can be patterned into narrow ribbons, graphene nanoribbons (GNRs), and so the carriers are confined to a quasi-one-dimensional (1D) system. Similar to carbon nanotubes (CNTs), GNRs are classified into two types: zigzag-edge GNRs (ZGNRs) and armchair-edge GNRs (AGNRs). Calculations based on tight binding predict that ZGNRs are always metallic, while AGNRs can be either metallic or semiconducting, depending on their width. However, recent density functional theory calculations show that AGNRs are semiconducting, with an energy gap scaling with the inverse of the GNR width.[2] ZGNRs are also semiconductors with two localized electronic edge states,[3] which may become half-metallic when subjected to an external transverse electric field.[4] This opens the possibility of graphene-based spintronic applications. AGNRs, however, exhibit semiconducting behavior with an extremely low carrier effective mass, making them potential candidates for novel channel materials in the next generation field-effect-transistors[5–8] and integrated circuits.[9] Bandgap oscillations have also been predicted for semiconducting narrow armchair ribbons as the ribbon width varies.[10] These bandgap oscillations make it possible to tailor the electronic structure of graphene. Due to the weak spin-orbital coupling, graphene has been suggested to be an ideal material for spintronic applications, such as spin field-effect transistors. Ohishi *et al.*[11] demonstrated spin injection into a graphene thin film (GTF) with high reliability by employing a "non-local" four-terminal measurement scheme. Abanin *et al.*[12] observed a large nonlocal response near the Dirac point in fields as low as 0.1 T, which persisted up to room temperature, and found that graphene could effectively conduct electron spin. The study also showed that the spin current in graphene was stronger and easier to control than in some other materials. Therefore, graphene is expected to become the next generation spin-based electronic material.

Originally, people believed that GNRs would be more difficult to manufacture than CNTs. Making GNRs using lithographic,[13–15] chemical,[16–19] or sonochemical[20] methods is indeed challenging[21] and cannot be used for large-scale manufacturing with controllable width. Recently, however, many new methods have been developed. Very narrow (10–20 nm widths) graphene nanoribbons with smooth edges were fabricated successfully by longitudinally unzipping carbon nanotubes.[21,22] Parallel graphene ribbons with widths reaching several microns have been made by converting pre-patterned graphite belts, and the gaps between parallel graphene ribbons could reach a size comparable to the width of the ribbons.[23] The other methods that have demonstrated successes of manufacturing graphene patterns or ribbons include mask lithography,[24] transfer printing,[25] and laser- or ion-beam direct-writings.[26] In particular, graphene nanogap electrodes with gap width below 10 nm have been fabricated by atomic force microscopy (AFM) nanolithography.[27] These advances in technology allow the fabrication of microscale and nanoscale features readily achievable, paving the way of integrating all-carbon electronics in the semiconductor industry.[28]

With continued shrinkage of device size in microchips, lateral in-plane coupling (LIPC) between neighboring materials or devices becomes increasingly important. Currently, theoretical studies on GNR are mainly on isolated GNR and layered GNRs,[29,30] and the effects of LIPC, which is different from inter-layer coupling,[31] between lateral parallel GNRs have been rarely investigated. So far, we have not found another report on effective coupling distance between lateral parallel GNRs. In this work, we carry out a

a)Electronic mail: xqdai@henannu.edu.cn. Also at Department of Physics, Zhengzhou Teachers College, Zhengzhou, Henan 450044, People's Republic of China.

first-principle investigation using spin-polarized density functional theory (spin-polarized DFT), unveiling the electronic and magnetic properties of lateral coupled GNRs without hydrogen passivation. The effect of the inter-ribbon displacement (IRD) along the ribbon direction on the inter-ribbon LIPC is examined, and such coupling may be significant in the fabrication of GNRs for nanoelectronic devices.

II. MODELS AND METHODS

The calculations were performed within the framework of generalized-gradient approximation (GGA), as implemented within the Vienna Ab-initio Simulation Package (VASP),[32,33] employing projector augmented wave (PAW) potentials. The Kohn-Sham orbitals were expanded in plane waves with a relatively high energy cutoff of 460 eV. We found no significant change in the structural parameters if the energy cutoff was increased to 500 eV.

The GNR was modeled based on the calculated lattice constant (a = 2.468 Å), and a 15 Å vacuum layer was employed to separate neighbor graphene layers. The widths of the 8-ZGNR and 14-AGNR are $w_Z = 6.35\,a$ and $w_A = 6.5\,a$, respectively, where, by convention,[19,34] the 8-ZGNR denotes a zigzag-edged GNR with 8 zigzag chains in width and the 14-AGNR denotes an armchair-edged one having 14 dimer lines across the ribbon width (see Fig. 1). The choice of the ribbon width

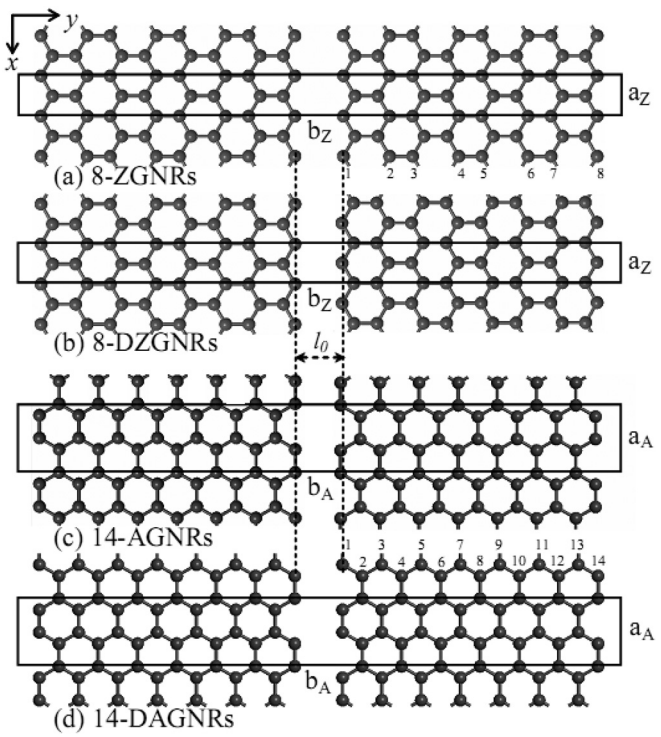

FIG. 1. Geometry of graphene ribbons separated by a spacing of l_0 perpendicular to the direction of the ribbon edge. The ribbons have finite width in the y direction and are assumed to be infinite along the x direction. The solid rectangles shows the supercell with length a_Z (a_A) and b_Z (b_A) in the x and y direction for ZGNRs (AGNRs), respectively. Here, the GNRs, which are single-layer and coplanar, are laterally parallel to each other. There is an IRD of $a_Z/2$ and $a_A/2$ along the x direction between two adjacent ribbons in the assembled structures (b) and (d) in comparison with that in structures (a) and (c), respectively.

was based on our test results that interedge coupling in such a ribbon is negligible. Different nanogaps between graphene ribbons were examined by setting different initial inter-ribbon distances l_0 in the calculations. l_0 is defined as the distance between the two parallel dashed lines shown in Fig. 1, which pass through the two outermost rows of atoms. There could also be a displacement of the two adjacent GNRs by $a_Z/2$ ($a_A/2$) along the ribbon direction (x in Fig. 1) for 8-DZGNRs (14-DAGNRs) [Fig. 1(b) and 1(d)] relative to that of 8-ZGNRs (14-AGNRs) [Fig. 1(a) and 1(c)]. Here, $a_Z = a$ and $a_A = \sqrt{3}a$. Considering such inter-ribbon displacements, two ribbons are included in the supercell, i.e., $b_Z = 2(l_0 + w_Z)$ and $b_A = 2(l_0 + w_A)$. In the calculation, four rows of the outermost edge atoms in the ribbons were allowed to relax and the force tolerance was set to be 0.03 eV/Å. Monkhorst-Pack grids of $(5 \times 1 \times 3)$ were employed to sample the Brillouin zone. A test showed that further increasing the number of k-points only led to an energy change of less than 0.5 meV.

III. RESULTS AND DISCUSSIONS

A. Effects of inter-ribbon LIPC on ZGNRs

1. Atomic structure and charge density

The atomic structures of the 8-ZGNRs and 8-DZGNRs with different initial inter-ribbon distance l_0 have been studied. After optimization, there is a change of the inter-ribbon spacing, and the magnitude of change $\Delta l = l - l_0$ is plotted in Fig. 2(a). Figure 2(b) shows the corresponding energy E. It is found that there are damped oscillations both in Δl and in E with changing l_0. This is in good agreement with the previous theoretical result that the inter-ribbon tensile stress exhibits a damped oscillation with increasing inter-ribbon distance.[35] Considering the symmetries of the ZGNR and DZGNR systems, the atomic configurations of the systems are given in Figs. 2(c)–2(f). When l_0 is very small (≤ 3 Å), the edge atoms in two ZGNRs move close to each other and the two ribbons combine into one. On the other hand, for $l_0 > 10$ Å, invariable Δl and E indicate the interaction between ribbons becomes negligible. So the most interesting and variant interactions between GNRs are those where their separations l_0 are in the range of 3 to 10 Å. Also shown in Fig. 2(b) is the insensitivity of the energy to inter-ribbon displacement when l_0 is greater than 5 Å, as ZGNRs and DZGNRs display the same energy for $l_0 > 5$ Å. In other words, the effect of IRD on LIPC between ZGNRs is insignificant when they are widely separated.

The inter-ribbon distance influences strongly, however, on atomic structure and charge density distribution in nanoribbons when $l_0 < 5$ Å. Charge density plot of ZGNRS with $l_0 = 3$ Å [Fig. 2(c)] shows that the edge atoms in the two ribbons form C–C bonds. The C–C bonds' lengths, in the perpendicular direction to the ribbon, are increased from the ideal 1.43 Å for graphene to 1.67 Å, while the other bond lengths are almost unaltered. Similar results were not found for DZGNRs with $l_0 = 3$ Å [Fig. 2(d)]. Rather, there is an obvious space between two ribbons after optimization. Thus, the IRD significantly affects the charge distribution near the edges when the initial inter-ribbon distance is less than 5 Å.

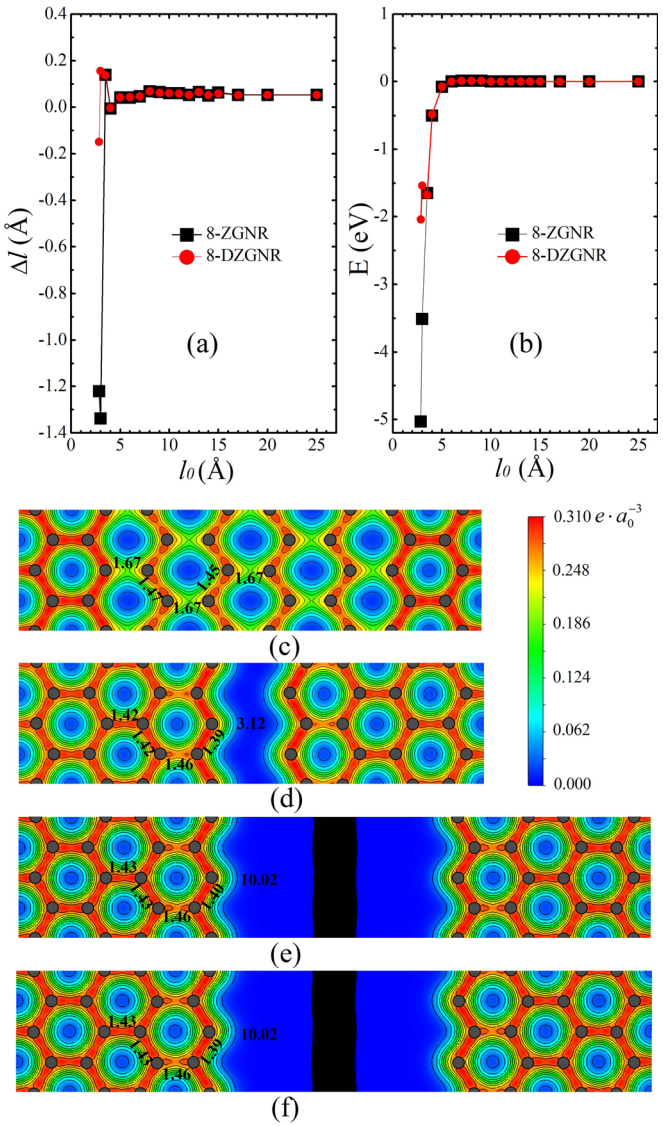

FIG. 2. (Color online) (a) The difference between the inter-ribbon distances before and after optimization and (b) the total energy of 8-(D)ZGNRs with the different initial inter-ribbon distances l_0. The total energy of the system with $l_0 = 15$ Å is set as the reference point for energy. Atomic structure and charge density distribution of 8-ZGNRs (c, e) and 8-DZGNRs (d, f) systems with different l_0: 3 Å (c, d) and 10 Å (e, f). Here, Angstrom is used as the unit of length, the charge density is drawn from the graphene plane, and a common scale is adopted. The symbol a_0 denotes the Bohr radius, and the black balls represent C atoms, similarly hereinafter.

2. Spin density

The distributions of electron spin polarization and local magnetic moment of the two types of coupled GNRs (ZGNRs and DZGNRs) with different inter-ribbon distances have been calculated and the results are shown in Fig. 3. From the figure, it is found that the magnetic moments are strongly localized at the zigzag edge sites. In the Bader analysis, the moment per C atom manifests exponential decay from the edge to the center of the ribbon. For the system of ZGNR with $l_0 = 6$ Å, the local magnetic moment of a C atom located at the utmost edge is 1.13 μ_B and the magnetic moment provided by the utmost edge atoms is accounting for 87.9% of the total magnetic moment. The inter-ribbon distance and the IRD along the ribbon direction hardly affect

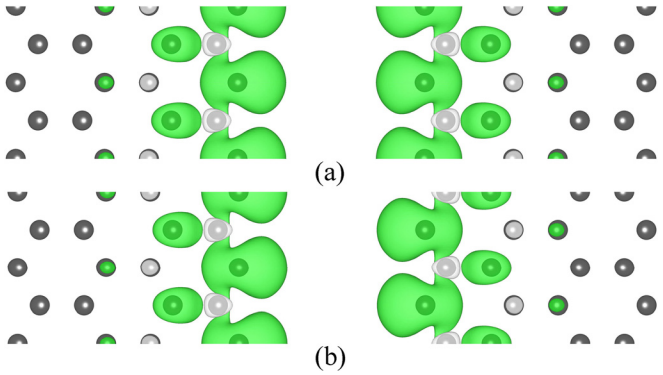

FIG. 3. (Color online) Spin density distribution for (a) the 8-ZGNRs (b) the 8-DZGNRs with $l_0 = 6$ Å. The dark (green) and light (gray) isosurfaces $(4.0 \times 10^{-2} \mathrm{e} \cdot a_0^{-3})$ in the images represent the spin-up and spin-down spin densities, respectively.

the spin distributions in the coupled ZGNRs when l_0 is greater than 5 Å.

3. Energy band structure

The spin-polarized electronic energy bands of (D)ZGNRs are shown in Fig. 4. The energies are measured relative to the Fermi level. There is a shift between the up- and down-spin subbands, which results in the net magnetic moment of the system. The shift derives from the 2 p electron spin polarization of C atoms near the edges. The up- and down-spin edge states U_Z and D_Z are situated below and above the Fermi level, respectively. Since the edge states U_Z and D_Z form flat bands, they situate on both sides of the Fermi energy (E_F) and give rise to large density of states peaks at E_F. Unlike the case of two-dimensional graphene with a zero density of states at E_F, infinitesimally small on-site repulsions in ZGNRs could make the latter magnetic.[19]

When $l_0 \geq 10$ Å [Fig. 4(f)], edge state U_Z is split into two states U_{Z1} and U_{Z2} below the Fermi level at the Gamma point (Γ). The two states are all twofold degenerate and located about 1.71 eV and 1.74 eV below the Fermi level, respectively. The energy band splitting at Γ remained at ~0.03 eV. Comparing with our calculations of single ZGNR, the energy band splitting (U_Z splits into U_{Z1} and U_{Z2} when $l_0 \geq 10$ Å) may be caused by the Ruderman-Kittel–Kasuya–Yosida (RKKY)-like interaction[36] as mediated by π electrons between two edges of ZGNR. There is no interaction between two zigzag graphene nanoribbons when $l_0 \geq 10$ Å, which is in agreement with the conclusion from the total energy of systems.

When $l_0 = 9$ Å [Fig. 4(e)], U_{Z1} (U_{Z2}) is split into two states U_{Z1a} and U_{Z1b} (U_{Z2a} and U_{Z2b}) and has a small energy splitting of about 1 meV at Γ. This indicates the weaker inter-ribbon interaction. With the decrease of l_0, energy splitting of U_{Z1} (U_{Z2}) becomes increasingly apparent. The splitting is 34 meV (35 meV) for U_{Z1} (U_{Z2}) when $l_0 = 6$ Å [Fig. 4(c)]. For $l_0 = 4$ Å [Fig. 4(b)], energy splitting of the spin-up (spin-down) edge state at Γ is found to be 0.54 eV (0.87 eV) and the splitting extends from Γ to X. For the ZGNRs, due to the ferrimagnetic spin texture near the edge, two counterproductive spin-spin interactions act on them and

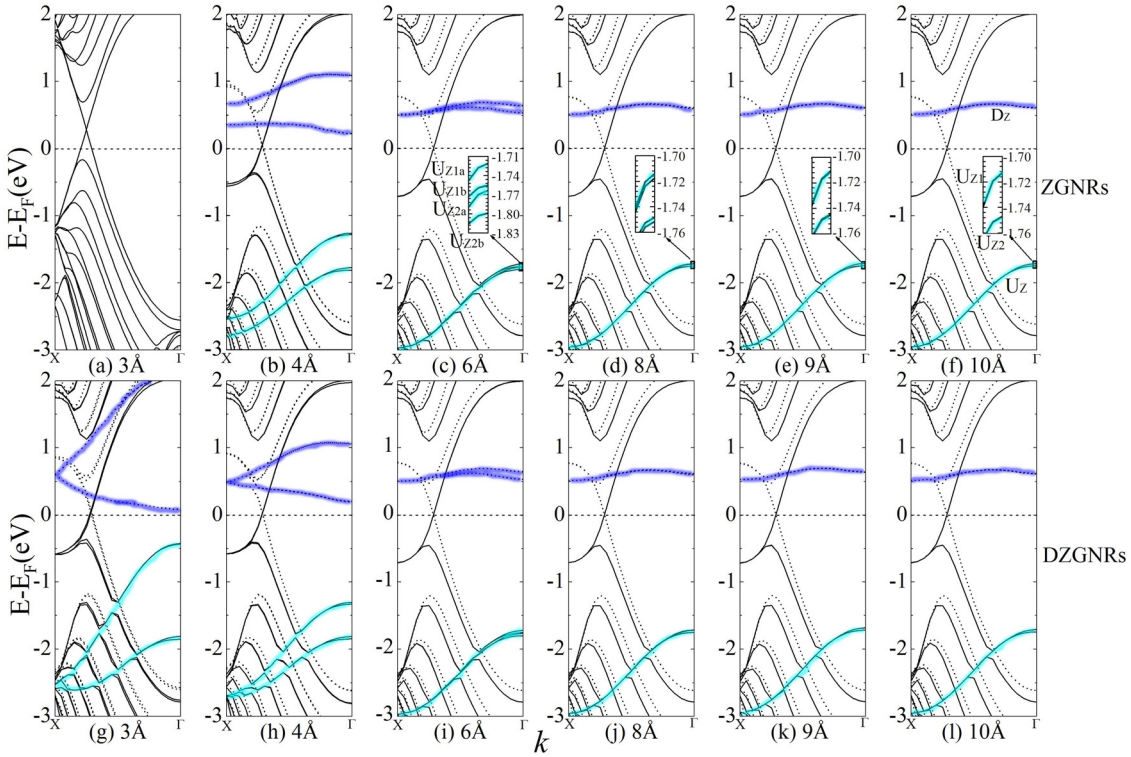

FIG. 4. (Color online) Spin-up (solid curves) and spin-down (dotted curves) energy-band structure of 8-ZGNRs with initial inter-ribbon distance $l_0 = 3$ Å (a), 4 Å (b), 6 Å (c), 8 Å (d), 9 Å (e), 10 Å (f) and 8-DZGNRs with $l_0 = 3$ Å (g), 4 Å (h), 6 Å (i), 8 Å (j), 9 Å (k), 10 Å (l), respectively. The insets are magnified plots of the less energy regions in plots (a), (c), and (e)-(f). Dashed lines represent the Fermi energy and $E_F = 0$. The up- and down-spin edges states U_Z and D_Z are located below and above the Fermi level, respectively.

give rise to the splitting of edge state when two ribbons are laid closely. The spin-spin interaction between the ribbons is a contributory cause of the band splitting besides the Coulomb interaction between ribbons. In the case of $l_0 = 3$ Å, the coupled ZGNRs are actually transformed into partially strained graphene, which shows the metal characteristics [See Fig. 4(a)]. The strained segments resemble extended defects in graphene as a metallic wire.[37] It is different from the case of wholly strained graphene with a tunable energy gap.[38]

As shown in Fig. 4(g)–4(l), the initial inter-ribbon distance l_0 (in the range of 3 to 9 Å) influences the energy band structure of the DZGNRs system. The splitting of edge states widens dramatically from 1 meV at $l_0 = 9$ Å [Fig. 4(k)] to about 1.41 eV at $l_0 = 3$ Å [Fig. 4(g)]. When l_0 is more than 10 Å, the constant band splittings suggest the interaction between the ribbons can be negligible. From energy band structures of ZGNR and DZGNR, it is found that the IRD affects the energy band structure of ZGNRs only when l_0 is less than about 5 Å.

B. Effects of inter-ribbon LIPC on AGNRs

1. Atomic structure and charge density

In this section, the inter-ribbon LIPC properties of AGNRs are investigated. Being similar to the case of ZGNRs, the change of inter-ribbon distance Δl and the total energy E exhibit damped oscillations with the increase of the inter-ribbon distance l_0. When l_0 is greater than 5 Å, Δl and E remain relatively constant. Structural optimizations show that the C–C bond lengths at the edge are about 1.25 Å. It is believed that the charge redistribution near the edges of armchair ribbons results in the formation of strong C–C covalent bonds that are close to C–C triple bonds. In addition, only when the initial inter-ribbon distance is very small ($l_0 \leq 3$ Å) would the weak electron-spin polarize, giving rise to a very feeble magnetization ($\sim 0.07\ \mu_B$/supercell) in C atoms at the edge. The electron spin polarization is not observed in the AGNRs when l_0 is greater than 3 Å. The spin-spin interaction between adjacent ribbons is negligible. This may be one of the reasons that the critical coupling distance in AGNRs is smaller than that in ZGNRs.

2. Energy band structure

Figure 5 depicts the energy band structure of the 14-AGNRs and 14-DAGNRs with some specific inter-ribbon distances ($l_0 = 3$ Å, 4 Å, 5 Å, and 6 Å). In the case of $l_0 = 3$ Å [Fig. 5(a)], the system of AGNRs presents metallic behavior because the edge state and π state pass through the Fermi level near X and Γ points, respectively. Like the vacancy defects,[37,39] the narrow nanogap with the armchair edges in graphene resembles an extended metallic wire in the graphene sheet. For $l_0 > 3$ Å [Fig. 5(b)–5(d)], AGNRs show semiconductor behaviors with tunable indirect energy gap by changing the width of the inter-ribbon gap, which increases from 0.20 eV at $l_0 = 4$ Å to 0.34 eV at $l_0 = 5$ Å), and 0.38 eV for $l_0 > 5$ Å (Table I). The effects of IRD on the energy gap of the system are negligible when $l_0 > 5$ Å. There is a direct-to-indirect band-gap transition when l_0 is increased from 4 to 5 Å for DAGNRs.

Except for $l_0 = 3$ Å, the up- and down-spin states are degenerate for the system of 14-AGNRs. Edge states S_{A1} and

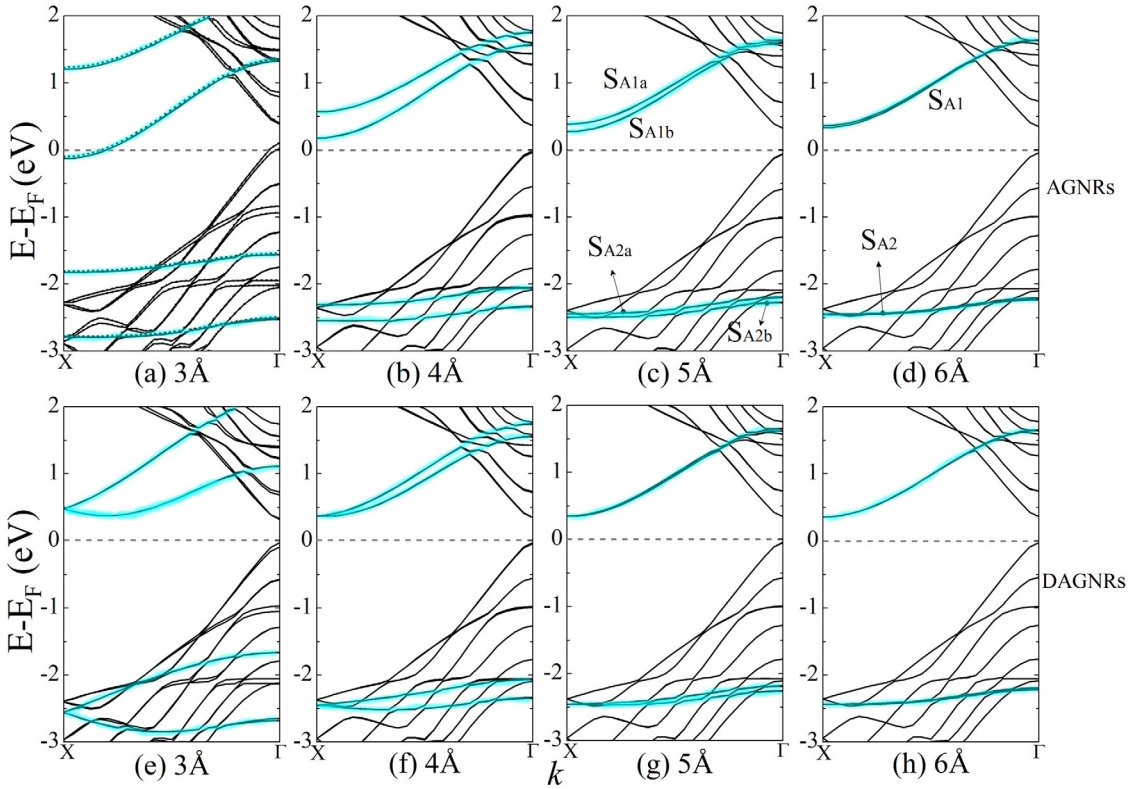

FIG. 5. (Color online) Energy-band structure of 14-AGNRs with $l_0 = 3$ Å (a), 4 Å (b), 5 Å (c), 6 Å (d), and 14-DAGNRs with $l_0 = 3$ Å (e), 4 Å (f), 5 Å (g), 6 Å (h), respectively. Except for AGNRs with $l_0 = 3$ Å [spin-up (solid curves) and spin-down (dashed curves)], the up-and down-spin states are degenerate for all the other systems mentioned here. Dashed lines represent Fermi energy and $E_F = 0$. Edges states S_{A1} and S_{A2} are located above and below the Fermi level, respectively.

S_{A2} are located above and below the Fermi level, respectively. When l_0 is less than 6 Å, the state S_{A1} (S_{A2}) is split into S_{A1a} and S_{A1b} (S_{A2a} and S_{A2b}). Unlike the edge state splitting in ZGNRs, the splitting of the state S_{A1} is almost the same from Γ to X in AGNRs with $l_0 < 6$ Å. This may be due to the fact that the C–C bonds at the edge are parallel to the armchair nanoribbon edge (x axis in Fig. 1) For $l_0 \geq 6$ Å, however, the edge-state splitting disappears and the energy band structure is unchanged with increasing l_0. So inter-ribbon interaction is negligible. After undergoing IRD with $a_A/2$ along the ribbon direction, the occupied (unoccupied) edges states S_{A2a} and S_{A2b} (S_{A1a} and S_{A1b}) are degenerate at the X points, while the edges states remain split at Γ when $l_0 < 5$ Å. This comes from the variation of the system symmetry after the displacement. The inter-ribbon distance affects the energy band structure of AGNRs when l_0 is less than 6 Å. The edge-state splitting decreases with the increase of the inter-ribbon distance. When l_0 is more than 6 Å, there are no changes in the energy band structures with changing inter-ribbon distances and the interaction between the ribbons could be neglected. The spin-spin interaction is not found between the edge atoms of the AGNRs. This may be one of the reasons that the coupling distance of the AGNRs is smaller than that of ZGNRs.

TABLE I. The band gap E_g^A (E_g^{DA}) of 14-AGNRs (14-DAGNRs) with the different inter-ribbon distance l_0. The result marked with a superscript "*d*" means that it is "direct" band gap; otherwise, "indirect" one.

l_0 (Å)	3	4	5	6	7	8	9	≥10
E_g^A (*eV*)	Metallic	0.20	0.34	0.38	0.38	0.38	0.38	0.38
E_g^{DA} (*eV*)	0.35^d	0.38^d	0.39	0.39	0.39	0.39	0.39	0.38

IV. CONCLUSIONS

The first-principle plane wave pseudopotential method has been employed to study the electronic and magnetic properties of lateral in-plane coupled GNRs. With the increase of inter-ribbon distance, the total energy exhibits a degenerative oscillation for the modeled systems. The underlying physics can be ascribed to Coulomb interaction and spin-spin coupling between ZGNRs, while only Coulomb interaction is operative in AGNRs. When the initial inter-ribbon distance is greater than 10 Å (6 Å) for ZGNRs (AGNRs), the total energies reach a constant value. Energy band of the GNRs with small inter-ribbon distance shows that the LIPC will result in edge-state band splitting. This indicates that LIPC should be considered in lateral parallel GNRs with small inter-ribbon distances, but the coupling is negligible when the inter-ribbon distance exceeds 10 Å (6 Å) for ZGNRs (AGNRs). The LIPC between ZGNRs is stronger than that between AGNRs, and the spin-spin interaction between the edge atoms of the ZGNRs may be one of the factors. The inter-ribbon displacement along the ribbon direction influences the energy band structure of GNRs only when the initial inter-ribbon distance is less than 5 Å. This study may provide predictive theoretical guidance to fabrication of graphene-based nanoelectronics and spintronic devices in the future.

ACKNOWLEDGMENTS

This research work has been supported by the National Natural Science Foundation of China (NSFC) under Grant No. 11047026 and Henan Science and Technology Innovation Talent Support Program (2008HASTIT030).

[1]K. S. Novoselov, A. K. Geim, S. V. Morozov, D. Jiang, Y. Zhang, S. V. Dubonos, I. V. Grigorieva, and A. A. Firsov, Science **306**, 666 (2004).
[2]V. Barone, O. Hod, and G. E. Scuseria, Nano Lett. **6**, 2748 (2006).
[3]L. Pisani, J. A. Chan, B. Montanari, and N. M. Harrison, Phys. Rev. B **75**, 064418 (2007).
[4]Y. W. Son, M. L. Cohen, and S. G. Louie, Nature **444**, 347 (2006).
[5]B. Obradovic, R. Kotlyar, F. Heinz, P. Matagne, T. Rakshit, M. D. Giles, M. A. Stettler, and D. E. Nikonov, Appl. Phys. Lett. **88**, 142102 (2006).
[6]X. Liang, Z. Fu, and S. Y. Chou, Nano Lett. **7**, 3840 (2007).
[7]G. Fiori and G. Iannaccone, IEEE Electron Device Lett. **28**, 760 (2007).
[8]X. Wang, Y. Ouyang, X. Li, H. Wang, J. Guo, and H. Dai, Phys. Rev. Lett. **100**, 206803 (2008).
[9]Y. M. Lin, A. Valdes-Garcia, S. J. Han, D. B. Farmer, I. Meric, Y. Sun, Y. Wu, C. Dimitrakopoulos, A. Grill, P. Avouris, and K. A. Jenkins, Science **332**, 1294 (2011).
[10]M. Ezawa, Phys. Rev. B **73**, 45432 (2006).
[11]M. Ohishi, M. Shiraishi, R. Nouchi, T. Nozaki, T. Shinjo, and Y. Suzuki, Jpn. J. Appl. Phys. **46**, L605 (2007).
[12]D. A. Abanin, S. V. Morozov, L. A. Ponomarenko, R. V. Gorbachev, A. S. Mayorov, M. I. Katsnelson, K. Watanabe, T. Taniguchi, K. S. Novoselov, L. S. Levitov, and A. K. Geim, Science **332**, 328 (2011).
[13]Z. Chen, Y. M. Lin, M. J. Rooks, and P. Avouris, Physica E **40**, 228 (2007).
[14]M. Y. Han, B. Özyilmaz, Y. Zhang, and P. Kim, Phys. Rev. Lett. **98**, 206805 (2007).
[15]L. Tapasztó, G. Dobrik, P. Lambin, and L. P. Biró, Nat. Nanotechnol. **3**, 397 (2008).
[16]A. Ghosh, K. S. Subrahmanyam, K. S. Krishna, S. Datta, A. Govindaraj, S. K. Pati, and C. N. R. Rao, J. Phys. Chem. C **112**, 15704 (2008).
[17]L. Ci, Z. Xu, L. Wang, W. Gao, F. Ding, K. Kelly, B. I. Yakobson, and P. M. Ajayan, Nano Res. **1**, 116 (2008).
[18]J. Campos-Delgado, J. M. Romo-Herrera, X. Jia, D. A. Cullen, H. Muramatsu, Y. A. Kim, T. Hayashi, Z. Ren, D. J. Smith, Y. Okuno, T. Ohba, H. Kanoh, K. Kaneko, M. Endo, H. Terrones, M. S. Dresselhaus, and M. Terrones, Nano Lett. **8**, 2773 (2008).
[19]M. Fujita, K. Wakabayashi, K. Nakada, and K. Kusakabe, J. Phys. Soc. Jpn. **65**, 1920 (1996).
[20]X. Li, X. Wang, L. Zhang, S. Lee, and H. Dai, Science **319**, 1229 (2008).
[21]L. Jiao, L. Zhang, X. Wang, G. Diankov, and H. Dai, Nature **458**, 877 (2009).
[22]D. V. Kosynkin, A. L. Higginbotham, A. Sinitskii, J. R. Lomeda, A. Dimiev, B. K. Price, and J. M. Tour, Nature **458**, 872 (2009).
[23]C. Cong, T. Yu, H. Wang, K. Zheng, P. Gao, X. Chen, and Q. Zhang, Small **24**, 2837 (2010).
[24]C. Cong, T. Yu, Z. Ni, L. Liu, Z. Shen, and W. Huang, J. Phys. Chem. C **113**, 6529 (2009).
[25]M. J. Allen, V. C. Tung, L. Gomez, Z. Xu, L. M. Chen, K. S. Nelson, C. Zhou, R. B. Kaner, and Y. Yang, Adv. Mater. **21**, 2098 (2009).
[26]Y. Zhou, Q. Bao, B. Varghese, L. A. L. Tang, C. K. Tan, C. H. Sow, and K. P. Loh, Adv. Mater. **22**, 67 (2009).
[27]Y. He, H. Dong, T. Li, C. Wang, W. Shao, Y. Zhang, L. Jiang, and W. Hu, Appl. Phys. Lett. **97**, 133301 (2010).
[28]Y. Zhou and K. P. Loh, Adv. Mater. **22**, 3615 (2010).
[29]D. Finkenstadt, G. Pennington, and M. J. Mehl, Phys. Rev. B **76**, 121405 (2007).
[30]N. Kharche, Y. Zhou, K. P. O'Brien, S. Kar, and S. K. Nayak, ACS Nano **5**(8), 6096 (2011).
[31]Y. Sui and J. Appenzeller, Nano Lett. **9**(8), 2973 (2009).
[32]G. Kresse and J. Furthmüller, Phys. Rev. B **54**, 11169 (1996).
[33]G. Kresse and J. Hafner, Phys. Rev. B **47**, 558 (1993).
[34]Y. W. Son, M. L. Cohen, and S. G. Louie, Phys. Rev. Lett. **97**, 216803 (2006).
[35]Z. Xu and M. J. Buehler, Nanotechnology **20**, 375704 (2009).
[36]W. Li, M. Zhao, X. Zhao, Y. Xia, and Y. Mu, Phys. Chem. Chem. Phys. **12**, 13699 (2010).
[37]J. Lahiri, Y. Lin, P. Bozkurt, I. I. Oleynik, and M. Batzill, Nat. Nanotechnol. **5**, 326 (2010).
[38]Z. Ni, T. Yu, Y. Lu, Y. Wang, Y. Feng, and Z. Shen, ACS Nano **2**, 2301 (2008).
[39]X. Dai, J. Zhao, M. Xie, Y. Tang, Y. Li, and B. Zhao, Eur. Phys. J. B **80**, 343 (2011).